ARNOLD DIFFUSION IN MANY DIMENSIONS

by

B. P. Wood, A. J. Lichtenberg, and M. A. Lieberman

Memorandum No. UCB/ERL M93/13

8 February 1993

ELECTRONICS RESEARCH LABORATORY

College of Engineering
University of California, Berkeley
94720

ARNOLD DIFFUSION IN MANY DIMENSIONS

by

B. P. Wood, A. J. Lichtenberg, and M. A. Lieberman

Memorandum No. UCB/ERL M93/13

8 February 1993

ARNOLD DIFFUSION IN MANY DIMENSIONS

by

B. P. Wood, A. J. Lichtenberg, and M. A. Lieberman

Memorandum No. UCB/ERL M93/13

8 February 1993

ELECTRONICS RESEARCH LABORATORY

College of Engineering
University of California, Berkeley
94720

Arnold Diffusion in Many Dimensions

B. P. Wood, A. J. Lichtenberg, and M. A. Lieberman*
Department of Electrical Engineering and Computer Sciences
and the Electronics Research Laboratory
University of California, Berkeley, CA 94720

Abstract

When several standard maps are coupled together, KAM surfaces cannot isolate stochastic regions, and particles diffuse along stochastic layers by the process of Arnold diffusion. For the case of two coupled standard maps the rate of Arnold diffusion has previously been calculated both locally around a particular KAM curve and globally across many cells of the 2π periodic mapping. When more than two standard maps are coupled, the Arnold diffusion rate increases, depending on the total number of maps, N, and the number of phases in each coupling term, m, where $2 \leq m \leq N$. As N is increased, the diffusion rate increases as $N^{1/2}$, the length of the diagonal in the action space. As m is increased, the diffusion rate increases because the phase of the coupling term for a particular map becomes less correlated with the phase of the map itself. In the limit of large m, the coupling term is randomized with each iteration. When the effect of N is removed by dividing the diffusion distance $\Delta I_{\rm rms}$ by $N^{1/2}$, a global diffusion $\Delta I_{\rm rms}$ versus m is found which is determined by the effect of m on the local rate of Arnold diffusion and the relative volume occupied by the various stochastically accessible regions in the coupled phase space. For

* Currently at Los Alamos National Laboratory MS-E526, Los Alamos, NM 87545

local Arnold diffusion, the increase in $\Delta I_{\rm rms}$ for a particular m depends strongly on the stochasticity parameter K. An analytic calculation of this K dependence for the cases of two and three coupled maps and an analytic calculation for the m dependence at fixed K are presented, which are in good agreement with numerical results.

Dedication

We dedicate this paper on Arnold diffusion to our former colleague and friend, Jeff Tennyson. It is very fitting that the paper is about Arnold diffusion, as we first worked on the subject with Jeff when he was a graduate student in our group. Jeff was looking for a mechanism to explain the very puzzling phenomenon of beam blow-up of intersecting beams in storage rings and came up with Arnold diffusion as a possible mechanism. Taking a simple model for study his work led to the first calculation and numerical comparison of the diffusion in mappings. The work has stimulated our continued interest in this very fascinating universal instability of nonlinear Hamiltonian systems.

Jeff went on to look at beam blow-up in more detail, and concluded that dissipative mechanisms were a more likely cause of the phenomenon. However, his initial inclination to use a simple mapping model to study a complex process, illustrates an important characteristic of Jeff's approach to science. He was always searching for the most fundamental methods to describe physical phenomena. We shall all miss his stimulating questioning of our understanding. We shall also miss his kind nature and his friendship.

1 Introduction

In non-integrable Hamiltonian systems of more than two degrees of freedom, KAM curves cannot isolate the stochastic layers that lie along the separatricies of system resonances. Stochastic layers lie along an inter-connected web of resonances such that initial conditions in any part of the web can ultimately diffuse to all parts of it. The process, first proved to exist by Arnold [1] and now known as Arnold diffusion, has been studied in a variety of problems.

If three resonances can be locally isolated to be of dominant importance, then a method exists for calculating the rate of diffusion along a local resonance layer, known as the three resonance model [2] or the stochastic pump model [3]. The model has been used to analytically calculate the local diffusion rate for coupled maps [2, 3, 4], and for two coupled standard maps, in particular [5, 6], with good agreement obtained with numerical results. The three resonance model predicts $D = (\Delta I)^2/t \propto \mathrm{e}^{-A/\epsilon^{1/2}}$ where ϵ is the perturbation parameter and $A \approx 1$.

If many resonance layers overlap then the three resonance model is not adequate to describe the diffusion, which can be much larger than that calculated using a three resonance model. An upper bound on the diffusion rate has been obtained by Nekhoroshev [7] of the form $D \propto \mathrm{e}^{-A/\epsilon^{\gamma}}(A \approx 1)$ where for the number of degrees of freedom $\overline{N}$, $\gamma = \left(\frac{3}{4}(\overline{N}-1)\overline{N}+2\right)^{-1}$. By allowing a somewhat more restrictive Hamiltonian, but still encompassing most physical problems, this upper bound can be improved such that [8, 9]

$$D \propto e^{-A/\epsilon^\gamma}, \qquad \gamma \approx \overline{N}^{-1}. \tag{1}$$

Nevertheless, if $\overline{N}$ is large it is clear that such an exponentially small diffusion could only hold for very small ϵ, otherwise the exponential factor would be essentially unity. It should also be pointed out that an upper bound must be related to the fastest local diffusion. This may be much more rapid than an average global diffusion, which would be controlled by the portions of the phase space where the diffusion is slowest.

In a model problem in which many resonances overlap, for $\overline{N} = 3$, Chirikov et al. [10] numerically investigated the scaling of the diffusion with ϵ, finding that it agreed with (1) for ϵ small, while it followed the three resonance model $\gamma = 1/2$ for larger ϵ. However, the important $\overline{N}$-dependence was not investigated.

To investigate global diffusion it is useful to employ a system that has uniform properties in a coarse-grained sense. The standard map, described by the equations

$$\begin{aligned} I_{n+1} &= I_n + K \sin\theta_n, \\ \theta_{n+1} &= \theta_n + I_{n+1}, \qquad \mod 2\pi, \end{aligned} \tag{2}$$

where I is the action and θ is the phase, has this important property as it is 2π periodic in both angle and action. This latter property has been used for the study of diffusion in a single map [11, 4]. As can be seen in Figure 1, generated by iterating a number of initial conditions with stochasticity parameter $K = 0.8$, the phase space consists of regions of stochasticity (area filling trajectories) surrounding island chains of rational frequency. The regions of stochasticity are separated by

regular motion on phase-spanning KAM curves. The largest region of stochasticity (thick dark region), we refer to as the "primary stochastic region," and the thinner regions around smaller islands are "secondary stochastic regions." The KAM curves consist of two types, librational motion about fixed points (closed curves on the phase plane) and rotational motion (open curves spanning 2π in the phase θ). For $K \gtrsim 0.9716\ldots$ the final rotational KAM curve is destroyed, such that global diffusion in a coupled set of mappings is across resonances rather than Arnold diffusion along resources. Konishi and Kaneko [12] studied global diffusion in a set of coupled standard mappings of the form

$$p_i(t+1) = p_i(t) + \frac{K}{2\pi}\{\sin[2\pi(x_{i+1}(t) - x_i(t))] - \sin[2\pi(x_i(t) - x_{i-1}(t))]\},$$

$$x_i(t+1) = x_i(t) + p_i(t+1), \quad \text{mod } 1, \quad i = 1, 2, \ldots N.$$

This form of nearest neighbor coupling is analogous to the FPU oscillator chain that has been used to study the closely related problem of the approach to equilibrium in many degree of freedom systems [13, 14, 15]. Konishi and Kaneko investigated the diffusion for $0.2 \leq K \leq 1$, over a range of N values, and found for $N > 3$ that the diffusion coefficient D fitted an exponential with the power of $\epsilon \equiv K$ given by $\gamma \simeq 0.45$ and independent of N. This is quite different from the estimates obtained from the rigorous upper bounds, and is, in fact, close to $\gamma = 0.5$ predicted from a three-resonance model. However, the form of the mapping studied by Konishi and Kaneko does not distinguish how many resonances are driving the diffusion. A non-nearest neighbor coupling was also investigated, and the diffusion coefficient was fitted to a power law ϵ^γ finding $\gamma \approx 5$.

We have adopted an alternate procedure of linking simple standard maps together through a coupling term:

$$
\begin{aligned}
I^1_{n+1} &= I^1_n + K^1 \sin\theta^1_n + \mu \sin(\theta^1_n + \ldots + \theta^m_n), \\
\theta^1_{n+1} &= \theta^1_n + I^1_{n+1}, \bmod 2\pi, \\
&\vdots \\
I^N_{n+1} &= I^N_n + K^N \sin\theta^N_n + \mu \sin(\theta^N_n + \ldots + \theta^{m-1}_n), \\
\theta^N_{n+1} &= \theta^N_n + I^N_{n+1}, \bmod 2\pi,
\end{aligned}
\tag{3}
$$

where a total of N maps (the N is an index, not an exponent) are coupled together in groups of m, with $2 \leq m \leq N$. In other words, each map is coupled to itself and the next $m-1$ maps in cyclical order. Note that this system has $\overline{N} = N + 1$ degrees of freedom. In this form we leave the structure of the individual maps nearly unchanged by making the coupling strength μ small, and control the number of interacting resonances through the number of coupling phases. The nonlinearity parameters K^i, $1 \leq i \leq N$, can also be varied independently of the coupling.

Using this formalism we have investigated the diffusion for two coupled maps [5]. For two coupled maps the action space can be exhibited by plotting (in action) the crossings of a surface of section in the phases. Taking the surface at $\theta_1 = \theta_2 = \pi$, for parameters $K^1 = K^2 = 0.8$ and $\mu = 0.01$, in Figure 2 the positions of 10^3 particles are shown after 2×10^6 mapping iterations for each particle. The widths of the primary stochastic regions are shown in gray, and positions of a few other secondary stochastic regions are noted by lines, but their widths are not resolved. Although

not completely obvious from the figure, the positions of the particles are all in the connected web of stochasticity, some being in the thinner secondary layers (not shown). The region labeled A is a primary librational region in both maps, and the two regions labeled B are in a librational region of the period 2 island chain in one map and in a primary librational region in the other map. The regions on combinations of librational and rotational KAM curves in both maps are on KAM tori in the coupled map and hence are inaccessible from the stochastic web.

From the structure of a phase space divided between regular and chaotic motion it is evident that the fraction of the phase space volume on regular curves decreases with an increase in the number of degrees of freedom. We would expect, provided μ is small enough that the coupling does not greatly perturb the phase space of a single map, that the fraction of the volume of the coupled system occupied by KAM curves would scale as f^N, were f is the fraction of regular phase space in a single map. This would affect the diffusion rate if the initial conditions are placed randomly in the phase space, but not if the initial conditions are all placed within the stochastic web. If μ is not sufficiently small, then the coupling, itself, can be the primary determinant of the thickness of the secondary stochastic layers, as found in a previous study [5]. We will return to these questions in Section 2.

For $N = m = 2$, the local rms diffusion distance across rotational KAM curves has been previously derived to be [5]:

$$\Delta I_{\rm rms} = \frac{2\pi\mu\, n^{1/2} Q_0}{K_j^{1/4}\left[\frac{3}{2}\ln K_j + \frac{\pi^2}{K_j^{1/2}} - 4.27\right]^{1/2}} \frac{e^{\pi Q_0/2}}{\sinh(\pi Q_0)}$$
$$\approx 4\mu n^{1/2} Q_0 e^{-\pi Q_0/2} \tag{4}$$

where the particle is on the KAM curve with action I in the driven map and in the primary stochastic region of the driving map, which has a stochasticity parameter K_j. Q_0 is the ratio of the unperturbed rotational frequency ω_i of the driven map ($\omega_i = I_i$) to the linearized librational frequency $\omega_j = K_j^{1/2}$ about the fixed point of the driving map,

$$Q_0 = \frac{\omega_i}{\omega_j} = \frac{\omega_i}{K_j^{1/2}}, \tag{5}$$

where the subscript i and j refer to the driven and driving maps, respectively, and n is the number of iterations. The value of $\Delta I_{\rm rms}$ from (4) is plotted versus K_j in Fig. 3 (solid line), showing good agreement with the numerical values for $K_j \lesssim 0.9$. Each numerical value was determined for 2^{18} iterations of 256 particles started on a rotational KAM curve in the driven map, for $\mu = 10^{-4}$. Note that for $K_j \gtrsim 1.0$ the numerical values fall approximately on a line determined by choosing a random phase in the coupling term of the driven map (dashed line). This suggests a way to look at the local diffusion. Although the motion in the primary stochastic region is chaotic, there is a correlation between its phase and the phase of the driven map. This correlation is strongest for small K_j, in which the stochastic region is exponentially thin. At $K_j \approx 1.0$ the correlation time becomes comparable to a single iteration of the mapping, and the phase of the coupling term is effectively

randomized on every iteration. This interpretation suggests further that anything which randomizes the phase of the coupling term, such as coupling to additional maps, will increase the diffusion toward the random phase value. As we will shortly see, this is indeed the case.

The remainder of this paper is organized as follows. In Section 2 we consider the effect on the local diffusion of increasing the number of maps coupled together, and derive a value for the increase in diffusion in going from one to two driving maps. We use the result to develop a formalism for an arbitrary number of coupling phases. Then in Section 3 we examine the effect of coupling many maps on the global diffusion across the entire coupled phase space.

2 Local Arnold Diffusion in Many Coupled Maps

To explore the effect of the number of driving terms on the local diffusion, the driven map is coupled to all the driving maps, but the driving maps are not coupled to any other maps, as described by the equations

$$\begin{aligned}
I^1_{n+1} &= I^1_n + K_i \sin\theta^1_n + \mu \sin(\theta^1_n + \ldots + \theta^m_n), \\
\theta^1_{n+1} &= \theta^1_n + I^1_{n+1}, \\
I^2_{n+1} &= I^2_n + K_j \sin\theta^2_n, \\
\theta^2_{n+1} &= \theta^2_n + I^2_{n+1}, \\
&\vdots \\
I^m_{n+1} &= I^m_n + K_j \sin\theta^m_n, \\
\theta^m_{n+1} &= \theta^m_n + I^m_{n+1}.
\end{aligned} \tag{6}$$

This allows us to isolate the effect of adding additional phases into the coupling term while not permitting the driving maps to drive each other out of their respective primary stochastic regions. For a fixed N, increasing the number $m-1$ of driving maps increases the rate of Arnold diffusion, as shown in Fig. 4, where we have plotted the local diffusion distance $\Delta I_{\rm rms}$ versus the number of driving maps for three values of K_j, the stochasticity parameter of the driving maps. In each curve of Fig. 4, the same value of K_j is used for all the driving maps. A very small value of $K_i = 0.1$ is used for the driven map to reduce the effect of nearby island chains. The value $\Delta I_{\rm rms}$ is that across the single driven map, determined for 2^{18} iterations of 256 particles with $\mu = 10^{-4}$ and $I_i = 2.35$.

The asymptotic part of the curves, i.e., the approach to the random phase value (dashed line) has been explored by plotting the normalized distance $(R - \Delta I_{\rm rms})/R$ between $\Delta I_{\rm rms}$ and the random walk distance $R = \left(\frac{\mu^2}{2} \cdot 2^{18}\right)^{1/2}$, versus $m-1$, as given in Fig. 5. The asymptotic results fit reasonably well to a single empirical function of $m-1$ and K, the straight lines being determined by the relation

$$\Delta I_{\rm rms} = R\left(1 - \alpha e^{-\beta K^2 (m-1)}\right), \tag{7}$$

with $\alpha \approx 1.1$ and $\beta \approx 1.5$. The fit breaks down for small $m-1$ where an asymptotic value is inappropriate, and also for large $m-1$ where the variability of the numerically calculated diffusion does not allow $R - \Delta I_{\rm rms}$ to be determined.

Of fundamental importance for understanding the effect of an increased number of coupling terms is the calculation of the increase in local diffusion when we go from one to two driving maps. Consider a model in which each driving map individually

delivers kicks to the driven map. We see that the doubly driven map effectively receives kicks at twice the rate of the singly driven map. Since the two driving maps are not correlated (they are not coupled together) the mean square local diffusion rate doubles. Occasionally by chance, the two driving maps are approximately in phase, and deliver a single large kick to the driven map. These two effects are added to give the total increase in the diffusion rate.

We combine these two effects in the following calculation. The mean square size of the kick per half revolution along the separatrix of the primary stochastic region of a single driving map is proportional to the square of a Melnikov-Arnold integral [4]:

$$A_2 = \int_{-\infty}^{\infty} \cos[Q_0 s + \phi(s)] ds, \tag{8}$$

where $s = \omega_j t$ is a non-dimensional time, Q_0 is the ratio of rotational driven frequency to driving frequency, as defined in (5), and

$$\phi(s) = 4 \text{ atan } (e^s) - \pi \tag{9}$$

is the evolution of the angle along the separatrix. For two driving maps, we alter (9) to

$$\phi(s) = 4 \left[\text{atan } \left(e^{s+\theta/2}\right) + \text{atan } \left(e^{s-\theta/2}\right)\right] \tag{10}$$

Where θ is the phase difference between the two driving maps. Using (10) in (8), and integrating the result numerically gives the result plotted in Fig. 6 as a function of θ for $Q_0 = 3.71$, corresponding to $K_j = 0.4$. The large value of (8) when the two driving maps are in phase is evident. The oscillation of (8) away from $\theta \approx 0$

represents the effect of the two individual out-of-phase driving maps. We determine the range of θ to include in the calculation as follows: in (9), $\phi(s)$ represents motion on the separatrix of the primary stochastic region, so $\phi(s) \to \pm\pi$ as $s \to \pm\infty$. In reality, the particle in the primary stochastic region is not exactly on the separatrix, and so $\phi(s)$ oscillates irregularly between $\pm\pi$. The average period of this oscillation in $s = \omega_j t$ will be $\omega_j T$, where T is the average period (in mapping iterations) within the separatrix layer of the primary stochastic region [4]

$$T = \frac{2}{\omega_j} \ln \left| \frac{32\mathrm{e}}{w_1} \right|, \tag{11}$$

with $\omega_j \approx K_j^{1/2}$ and with

$$w_1 = 8\pi \left(\frac{2\pi}{K_j^{1/2}} \right)^3 \mathrm{e}^{-\pi^2/K_j^{1/2}} \tag{12}$$

the normalized thickness of the stochastic layer. Equations (11) and (12) combine to give

$$\omega_j T = \frac{2\pi^2}{K_j^{1/2}} + 2 \ln \frac{32\mathrm{e} K_j^{3/2}}{64\pi^4}. \tag{13}$$

The second term is negative, relatively small and slowly varying. For small values of K_j we can appropriate $\omega_j T \approx 2\pi^2 K_j^{-1/2}$. The procedure is then to take the ratio of the root mean square value of the entire curve in Fig. 6, taken over values of θ corresponding to one average period $\omega_j T$ of the oscillation in the stochastic layer, to the single phase Melnikov-Arnold integral. For the case of $K_j = 0.4$ ($Q_0 = 3.71$) shown in Fig. 6, using (13), the ratio of the mean square values is taken over approximately $\theta = s = \pm 3\pi$. Doing this yields a result for the diffusion enhancement factor which is plotted versus K_j as the solid line in Fig. 7. The values determined

by iterating the mapping are denoted by diamonds, showing reasonable agreement with the analytical result.

Consider now the procedure for going to more driving maps. We must sum the probabilities of the various kinds of interactions when one or more of the driving terms coincide to give one large kick. We develop a probabilistic formula and then analytically calculate the terms in the resulting sum. Taking the most general case of p driving phases, $d = r + s$ rotation and secondary stochastic phases, and ℓ libration phases ($m = p + d + \ell$), the local diffusion coefficient along any of the d actions $\mathbf{I} = (I_1, \ldots I_d)$ can be written in the form of a modified binomial expansion

$$D_{pd}(\mathbf{I}) = \frac{\mu^2}{2K_j T} \sum_{i=1}^{p} \binom{p}{i-1} \left(\frac{\Delta t}{T}\right)^{p-i} \left(1 - \frac{\Delta t}{T}\right)^{i-1} \times \frac{1}{\pi} \int_{-\frac{\pi}{2}}^{\frac{\pi}{2}} \cos^{2(p-i)} \theta' \, d\theta' A_{\mathrm{MA}}^2(p+1-i), \tag{14}$$

where T is obtained from (13), $T \approx 2\pi^2/K_j$, and $Q_d = \omega_d/K_j^{1/2}$, with $\omega_d = I_1 + I_2 + \cdots + I_d \bmod 2\pi$ for $0 < \omega_d < \pi$ and $\omega_d = 2\pi - [(I_1 + I_2 + \cdots + I_d) \bmod 2\pi]$ otherwise.

$A_{\mathrm{MA}}(k)$ is the peak value of the M-A integral for $k = p + 1 - i$ stochastic drives. For $\theta = 0$ in (10) we see that this coincides with the usual set of M-A integrals as defined in Refs. 2 and 4

$$A_{\mathrm{MA}}(k) = A_{2k},$$

where A_{2k} is determined by the recursion relation for MA integrals

$$A_\ell = \frac{2Q_0}{\ell - 1} A_{\ell-1} - A_{\ell-2}, \tag{15}$$

where $A_1 = 2\pi e^{\pi Q_0/2}/\sinh \pi Q_0$ and $A_2 = 2Q_0 A_1$. For large Q_0 this can be expressed in the closed form

$$A_\ell = \frac{(2Q_0)^{\ell-2}}{(\ell-1)!} A_2. \tag{16}$$

The binomial coefficients in (14) give the number of coincidences of the phases, that lead to the coincidence enhancement of the MA integrals. Specifically, the factor $(\Delta t/T)^{m-2}$ $(i = 1)$ is the probability of all $p-1$ enhancement peaks of width Δt occuring simultaneously within the interval T, and the integrals represent the sharpening of the peaks with increasing number of coincidences. The last $(i = p)$ term in (14) is due to the incoherent summing of the kicks of the p driving phases, and is a factor of two lower than the coherent sum of the two driving phases shown in the wings of Fig. 6, because of the incoherent summing of squared quantites. In (14), the effect of the ℓ libration phases on D_{pd} is neglected, which is valid in the limit of small K_j. The ratio of the peak of the MA integral with two driving phases, to the value of the single drive MA integral, for $K = 0.4$ $(Q_d = 3.7, A_{\rm MA}(1) = 0.278)$ is, from Fig. 6,

$$A_{\rm MA}(2)/A_{\rm MA}(1) \approx 8.$$

Using (15), we obtain $A_{\rm MA}(2)/A_{\rm MA}(1) = 7.8$, which is in agreement with this numerically determined ratio. This good agreement holds for all values of K. We also find that the width of the central maximum in the MA integral, $\Delta\theta = \omega_j \Delta t$, is proportional to $K_j^{1/2}$, with the actual width found numerically as in Fig. 6. The average total phase in the separatrix layer varies according to (13). The ratio $\Delta t/T$ as a function of K is given in Fig. 8. The integrals in (14) heuristically account

for the sharpening of the peak by additional coincidences and can be evaluated in closed form

$$\frac{1}{\pi}\int_{-\frac{\pi}{2}}^{\frac{\pi}{2}} \cos^{2k}\theta \; d\theta = \frac{(2k-1)!!}{2^k \; k!}. \tag{17}$$

Using these relations we plot in Fig. 9 the enhancement factor for $K_j = 0.2$ and $m-1$ between 1 and 5, corresponding to the numerical values found in Fig. 4. For comparison, we repeat the numerical results in Fig. 9. The theoretical curve (solid line) is in good agreement with the numerical values, indicating the essential correctness of the method. The enhancement of $\Delta I_{\rm rms}$ with increasing m follows closely the numerically determined enhancement.

3 Global Arnold Diffusion in Many Coupled Maps

We now examine the global diffusion in action across the higher dimensional phase space over long times. The N maps are coupled together in groups of m. As a special case, we choose the same value of K for every map. The distinction between driven and driving maps is lost, because a single map may be both driven and driving at different times in the diffusion process. For this reason, and because the diffusion rate varies greatly with the region of phase space a particle occupies, it should be noted that determining the global diffusion is a more complicated problem than determining the local diffusion.

We formulate an intuitive model of how the global diffusion proceeds. Assume a particle starts in the primary stochastic regions of all the maps (the intersections of the thickest shaded regions in Fig. 2). The particle will explore this multiple stochastic region, each map delivering kicks to the other maps, until it is kicked

out onto a nearby KAM curve in one or more of the maps (the thick shaded regions between intersections). The stochasticity in the remaining maps will then drive Arnold diffusion across these KAM curves (along the thick shaded regions). Eventually, the particle will encounter another stochastic region in one of the driven maps (one of the thinner shaded lines). The particle will then explore this stochastic region (the intersections of shaded lines), until it is again kicked out onto a nearby KAM curve to continue its Arnold diffusion (along one of the shaded lines). Occasionally the opposite happens and the kicks from a thin stochastic region will kick the particle out of a larger stochastic region in another map. It is by this process that the stochastic portion of the phase space will become populated. This process is elucidated with additional detail for two coupled maps in reference [5].

The dependence of the global rms Arnold diffusion distance $\Delta I_{\rm rms}$ on N and m is shown in Fig. 10, for $K = 0.8$, $\mu = 0.01$, and 2^{21} iterations of 256 particles. For each curve with a particular N, the diffusion distance approaches an asymptotic value with increasing m, as was the case for local diffusion. Larger values of N result in longer diffusion distances, because the phase space is larger. We can remove the effect of N by dividing each of the curves in Fig. 10 by $\sqrt{N}$, which is the length of the diagonal in the action space. The diffusion is then normalized to a single diffusing direction. The result, shown in Fig. 11, is that all that curves in Fig. 9 lie approximately on a universal curve, which is dependent only on m, with the exception of the points representing fully coupled sets of maps ($m = N$). These points lie along a lower curve, shown as the dotted line in Fig. 11, to which we have added the fully coupled cases for $N = 3$, 5, 6, and 7. We do not have an explanation

for why these points lie below the universal curve, although we speculate that additional correlation due to the symmetry is introduced when the coupling term has the same value for all maps, which is the case for a fully coupled system.

We now calculate a global diffusion for $N > 2$. We use the local diffusion coefficient (14) and phase space considerations. Our fundamental assumption is the ergodic assumption; that is, in the steady-state all accessible phase space is equally populated. To apply the assumption to a non-steady-state global diffusion problem we use the approximation that the more accessible portion of the phase space, which fills on the time scale required to calculate the diffusion, is sufficiently close to the total accessible phase space that a reasonably accurate calculation can be made. The hypothesis of asymptotic ergodicity has been checked for a simpler 2-D mapping [16]. Following the reasoning in reference [5], we assume that in a coupled map the primary stochastic region (which we will denote P) can drive Arnold diffusion across rotational orbits (R) and across the stochastic regions associated with the secondary resonances (S). It can also drive diffusion across a librational region (L), but this does not contribute to global diffusion because the motion averages to the location in action of the fixed point of a librational region. We determine the probabilities of a particle being in the various accessible regions of phase space, and the effect of the diffusion in each region.

Before considering the probabilities of the different types of phase space in which diffusion is taking place, we must first define appropriate averages over the diffusing (driven) direction. If there is only one regular phase in the coupling term, $d = r + s = 1$, which must then be the phase along the diffusing direction, then

the average diffusion coefficient $\overline{D}_{p1}$ for the diffusing action, say I, is obtained by averaging the reciprocal of $D_{p1}(I)$ over I

$$\frac{1}{\overline{D}_{p1}} = \frac{1}{\pi}\int_0^{\pi} \frac{dI}{D_{p1}(I)}.$$

D_p for stochastic orbits is large and librational orbits only store particles. Therefore we perform the average only over rotational orbits, yielding

$$\frac{1}{\overline{D}_{p1}} = \frac{1}{\pi}\int_R \frac{dI}{D_{p1,R}(I)}. \tag{18}$$

The form of $D_{p1,R}$ for the rotation orbits was given in reference [5]. Since the R and S regions are closely intermingled in action while $D_{p1,R}$ varies slowly over these regions, we can approximate (18) by

$$\frac{1}{\overline{D}_{p1}} = \frac{R}{R+S}\frac{1}{\pi}\int_{R+S} \frac{dI}{D_{p1,(R+S)}(I)}. \tag{19}$$

If there is more than one regular or secondary stochastic phase in the coupling term, $d \geq 2$, then these phases add to give a combined sum of actions $I_d = \omega_d$, as described previously. Since all values of action for the phases other than the diffusing phase are possible, an average must first be performed over these other actions. In this case

$$D_{p2}(I) = \int D_{p2}(\mathbf{I})\, d\mathbf{I}' \Big/ \int d\mathbf{I}' \tag{20}$$

where $\mathbf{I}'$ is an integration over all of the I's except the diffusing one, and the subscript $p2$ indicates that $d = r + s \geq 2$ in the coupling term. As discussed earlier, we assume that only actions in the R and S regions contribute, while the L actions are considered to oscillate about zero. To evaluate D_{p2}, we note that two or more

regular phases appear as a sum in the coupling term; hence, they can be considered as a single regular phase in evaluating the MA integral. This has been confirmed numerically. Performing the integral in (20) over the allowed ranges of all actions $\mathbf{I}'$ yields the result that $D_{p2}(I) = \text{const}$, independent of the diffusing (driven) action I. Performing the final average of D_{p2}^{-1} as in (19) to yield $\overline{D}_{p2}$ is then trivial.

In terms of $\overline{D}_{p1}$ and $\overline{D}_{p2}$, we can now express the global diffusion rate for m phases in the coupling and all mappings and couplings having the same form, as

$$D_g(N, m) = N\frac{R+S}{1-(R+L)^N}\sum_{p=1}^{m-1}\left\{\overline{D}_{p2}\binom{m-1}{p}P^p\left[(R+S+L)^{m-1-p} - L^{m-1-p}\right]\right.$$
$$\left. + \overline{D}_{p1}\binom{m-1}{p}P^p L^{m-1-p}\right\} \tag{21}$$

where, as previously $(R+S)$ is the fractional volume of the diffusing phase space, N is the number of maps in which diffusion can independently occur, P is the fractional volume of the phase space of the primary drive, and $1-(R+L)^N$ is the fractional volume of the accessible phase space. For N large, $D_g \propto N$, and thus $\Delta I_{\text{rms}} \propto N^{1/2}$, as found numerically.

We illustrate the method with a particular example, that of $K = 0.8$ for all maps and $\mu = 0.01$. This case has already been used to calculate the diffusion for two coupled maps, in reference [5]. The fractions of phase space in these various regions were found to be $P \approx 0.19$ primary stochastic, $S \approx 0.30$ secondary stochastic, $R \approx 0.11$ rotational, and $L \approx 0.40$ librational. To calculate the diffusion for two and three coupling phases we use the example of $N = 4$, so as to avoid the complications of a fully coupled system. (The subdivision of phase space is shown in Fig. 12 for

two coupled maps and one driving phase; $N = 2$, $m = 2$.) Using (21), the global diffusion is

$$D_g(4, 2) = 4\frac{P(R+S)}{1-(R+L)^4}\overline{D}_{11} \tag{22}$$

where the first subscript 1 indicates that $p = 1$. Since $d = 1$ (one regular phase), the first type of average (19) over the reciprocal of D_{11} is to be taken. Calculating $\overline{D}_{11}$ from (19), numerically,

$$D_{11} = 3.5 \cdot 10^{-5}. \tag{23}$$

Then, using (22) to calculate D_g, with the values of P, R, S, and L for $K = 0.8$, we have

$$D_g(4, 2) = 1.17 \cdot 10^{-5}. \tag{24}$$

To compare this theoretical result with the numerical value, we use

$$\Delta I_{\text{rms}} = (D_g n/N)^{1/2},\ (n = 2^{21},\ N = 4)$$

to find $\Delta I_{\text{rms}} = 2.5$ somewhat smaller than the numerical result in Fig. 11, as expected, because the numerics have not yet reached their asymptotic values [5].

We compare this with the result for three phases in the coupling. The global rate of diffusion for $N = 4$, $m = 3$ is given by the sum of the diffusion rates times their respective phase space volumes, each divided by the accessible volume. Using (21), we obtain

$$D_g(4, 3) = \frac{4(R+S)}{1-(R+L)^4}\left[P^2\overline{D}_{21} + 2P(R+S)\overline{D}_{12} + 2PL\overline{D}_{11}\right]. \tag{25}$$

The evaluation of $\overline{D}_{11}$ was given above. The evaluations of $\overline{D}_{12}$ and $\overline{D}_{21}$ are, in general, quite complicated. For the purposes of this comparison we will make some

simplifying assumptions. We assume that almost all frequencies (actions) associated with the second (non-diffusing) driving phase exist at each frequency (action) of the diffusing (driven) phase. Since the frequency in the MA integral is the sum of all the regular (rotational) frequencies, all actions of the driven phase have the same average and consequently the same average MA integral. This is obtained by averaging the MA integral over the driven phase. Explicitly, using A_2 as defined from (15), we can write

$$\overline{A}_{\mathrm{MA}} = \frac{1}{\pi}\int_0^{\pi} 4\pi Q_0 \frac{e^{\pi Q_0/2}}{\sinh(\pi Q_0)} dI, \tag{26}$$

where $Q_0 = I/K^{1/2}$. The integral has been evaluated numerically for $K = 0.8$ to give $\overline{A}_{\mathrm{MA}} = 3.1$. Using this average value of the MA integral, it is then trivial to evaluate (19) to calculate an approximate value of $\overline{D}_{12}$ as follows. Substituting $\overline{A}_{\mathrm{MA}}$ into (14) we only have a single term giving

$$D_{12} = \frac{\mu^2}{2KT}\overline{A}^2_{\mathrm{MA}} = 1.17 \cdot 10^{-5}$$

and from (19), we obtain

$$\frac{1}{\overline{D}_{12}} = \frac{R}{R+S}\frac{1}{\pi}\int_0^{\pi}\frac{dI}{D_{12}},$$

giving

$$\overline{D}_{12} = 3.6 \cdot 10^{-5}. \tag{27}$$

To find $\overline{D}_{21}$ we perform the average of $1/D_{21}$ as in (19), with the local D_{21} obtained directly from (14),

$$D_{21}(I) = \frac{\mu^2}{2KT}\left[\frac{1}{2}\frac{\Delta t}{T}A^2_{\mathrm{MA}}(2) + 2\left(1 - \frac{\Delta T}{T}\right)A^2_{\mathrm{MA}}(1)\right] \tag{28}$$

Numerically integrating (19), using (28), with the A_{MA} integrals obtained from (15) (note $Q_0 = I/K^{1/2}$), we obtain

$$\overline{D}_{21} = 1.5 \cdot 10^{-4}. \tag{29}$$

Substituting (23), (27) and (29) in (25), with values of P, $R+S$, and L obtained for $K = 0.8$, we have

$$D_g(4,3) = \frac{4(0.4)}{1-0.07}(0.04)1.5 \cdot 10^{-4} + (0.16)3.6 \cdot 10^{-5} + (0.16)3.5 \cdot 10^{-5} = 2.9 \cdot 10^{-5}. \tag{30}$$

Dividing by $D_g(4, 2)$ as given in (24) and taking the square root, we find the global enhancement factor

$$\frac{\Delta I_{\mathrm{rms}}(m=3)}{\Delta I_{\mathrm{rms}}(m=2)} \approx 1.6 \tag{31}$$

which is in reasonable agreement with the numerical enhancement factor of 1.9 obtained from Fig. 11.

4 Conclusions and Discussion

We have shown that the local Arnold diffusion in a system of coupled standard maps is enhanced as the number p of maps driving the diffusion is increased. For sufficiently large p the rms diffusion distance saturates at a value consistent with a random walk produced by randomizing the phase of the coupling term on every iteration. The number p of driving phases in the coupling term introduces two effects, a simple increase in the number of kicks by the number of stochastic driving terms, and an occasional large kick when two or more stochastic phases coincide. The latter effect dominates at small values of the stochasticity parameter K. We have calculated the diffusion enhancement factor as a function of the stochasticity

parameter K when the number of driving maps is increased from one to two, by generalizing the Melnikov-Arnold integral to include two driving phases. This approach was generalized to more driving phases, without performing the numerical integration, by assuming an analytic form of the MA integral that gives results in agreement with the numerical integration for two driving phases.

When the system diffuses globally, we have shown that the diffusion distance increases as the square root of the number of maps in the system. The global diffusion also saturates with increasing m for large m, which can be associated with the value at which the phase in the coupling term is randomized. A calculation of the global diffusion enhancement based on local diffusion enhancement and phase space volume considerations produces a result which is in reasonable agreement with numerical calculations. However, assumptions were made in the calculation that have not been checked in detail. Further work is necessary to confirm the relations as a function of the driving nonlinearity parameter K.

The scaling of K and p found in the local diffusion can be compared to the formulas bounding the diffusion from above. Because of the limit to the diffusion rate at the value at which the coupling phase is randomized on every mapping period, K must be kept sufficiently small with respect to m to see the proportionalities. We use (1), with $\epsilon = 1/Q_0^2$, $\gamma = 1/2\overline{N}$, and $A = \frac{\pi}{2}$, to match the exponent to the MA integral for $N = 2$ ($N = \overline{N} - 1$). We set the constant of proportionality to match $\Delta I_{\rm rms}$ at $N = 2$ ($m - 1 = 1$) in Fig. 8, and plot the fully coupled ($m = N$) scaling as a dashed line. The result lies everywhere above the calculated curve, as expected. However, we caution that we have not applied the "upper bound" formula for the sufficiently

small K to which it rigorously applies. This is quite difficult to do numerically, but is accessible from (14) and (15).

In a recent calculation Chirikov and Vecheslavov [17] have estimated that the rate of global diffusion for $\overline{N}$ sufficiently large and ϵ not too small behaves as a power law in ϵ, $D \propto \epsilon^{\eta}$, $\eta \approx 6.5$, and to be independent of $\overline{N}$. Since from (21), $D_g(N, m)$ saturates with increasing m, for a given K-value, the possibility is open of obtaining a power law variation of D with K. It is clear from the numerical results of Fig. 4 that the range over which such a formula could hold is limited, and not fully accessible with the numerical data. Equations (14), (15) and (21) can be used to extend the work into this power law regime, as described in the previous paragraph. We leave these comparisons for future work.

References

[1] V. I. Arnold. *Russian Mathematics Surveys*, 18:85 (1964).

[2] B. V. Chirikov. *Physics Reports*, 52:263 (1979).

[3] J. L. Tennyson, M. A. Lieberman, and A. J. Lichtenberg. In *Nonlinear Dynamics and the Beam-Beam Interaction, AIP Conference Proceedings No. 57*, page 272, New York (1979) American Institute of Physics.

[4] A. J. Lichtenberg and M. A. Lieberman. *Regular and Stochastic Motion.* Springer-Verlag, New York, (1983).

[5] B. P. Wood, A. J. Lichtenberg, and M. A. Lieberman. *Physical Review A*, 42:5885 (1990).

[6] G. R. Wang and B. Hu. *Physics Letters A*, 151:37 (1990).

[7] N. N. Nekhoroshev. *Russ. Math. Surv.*, 32:6 (1977).

[8] A. Giorgilli. *Ann. Inst. H. Poincare*, 48:423 (1988).

[9] P. Lochak. *Phys. Lett. A*, 143:39 (1990).

[10] B. V. Chirikov, J. Ford, and F. Vivaldi. *AIP Conf. Proc.*, 57:323 (1979).

[11] A. B. Rechester, M. N. Rosenbluth, and R. B. White. *Phys. Rev. A*, 23:2664 (1981).

[12] T. Konishi and K. Kaneko. *J. Phys. A*, 23:1715 (1990).

[13] E. Fermi, J. R. Pasta, and S. Ulam. *Collected Works of Enrico Fermi*, University of Chicago Press, Chicago, 1965. Studies of Nonlinear Problems.

[14] R. L. Bivins, N. Metropolis, and J. R. Pasta. *Journal of Computational Physics*, 12:65 (1963).

[15] R. Livi, M. Pettini, S. Ruffo, M. Sparpaglione, and A. Vulpiani. *Physical Review A*, 28:3544 (1983); *Physical Review A*, 31:1039 (1985).

[16] A. J. Lichtenberg and B. P. Wood. *Physical Review A*, 39:2153 (1989).

[17] B. V. Chirikov and V. V. Vecheslavov. "Theory of the Fast Arnold Diffusion in Many-Frequency Systems," Preprint, Budker Inst. of Nucl. Phys., Novosibirsk (1992).

Acknowledgement

The work was partly supported by National Science Foundation Grant ECS-8910762 and Office of Naval Research Grant N00014-89-J-1097. One of us (AJL) acknowledges useful conversations with Dr. S. Ruffo and Dr. R. Kapral, and the hospitality of Institute for Scientific Interchange, Torino, Italy.

Figure Captions

Figure 1. The standard map for $K = 0.8$ and a number of initial particle positions.

Figure 2. Arnold diffusion in the 2π periodic (I_1, I_2) phase plane for a surface of section at $\theta_1 = \theta_2 = \pi$, with $K^1 = K^2 = 0.8$ and $\mu = 0.01$. 1000 particles were started in the primary stochastic region of both maps, and run for two million iterations. The particles are superimposed upon a grid showing the primary stochastic region and the stochastic regions around the period 2, 3, and 4 island chains in the uncoupled map.

Figure 3. Local rms Arnold diffusion distance ΔI_{rms} versus K_j for two coupled maps. The solid line is the theoretical value. The dashed line represents the random walk value obtained by randomizing the phase of the coupling term on every iteration. The circles are the numerical calculations. ($\mu = 10^{-4}$, $n = 2^{18}$)

Figure 4. Local rms Arnold diffusion distance ΔI_{rms} versus $m - 1$ for three different values of K_j. The dashed line represents the random walk value obtained by randomizing the phase of the coupling term on every iteration.

Figure 5. Normalized difference between the local rms Arnold diffusion distance of Figure 4 and the random walk diffusion distance. The straight lines are an empirical fit.

Figure 6. The value of the Melnikov-Arnold integral versus the phase difference θ between two driving maps, for $K_j = 0.4$.

Figure 7. The local Arnold diffusion enhancement factor versus K_j. The points are determined from iterating the mapping, and the solid line is the theoretical value.

Figure 8. The ratio of Δt, the peak of the two-driving-phase Melnikov-Arnold integral, to the average period T of the separatrix layer, as a function of K.

Figure 9. Local rms Arnold diffusion distance versus $m-1$ for $K_j = 0.2$, compared to the theoretical prediction. The dashed line is a global "upper bound."

Figure 10. The global Arnold diffusion distance versus m for several values of N, the total number of maps ($K = 0.8$, $\mu = 0.01$, $n = 2^{21}$).

Figure 11. Same data as in Figure 10, but each curve has been normalized by dividing by $N^{1/2}$. The solid line is the universal curve. The dotted line is drawn through the data points representing fully coupled maps ($K = 0.8$, $\mu = 0.01$).

Figure 12. Phase space areas of the various regions of two weakly coupled maps; $K = 0.8$.

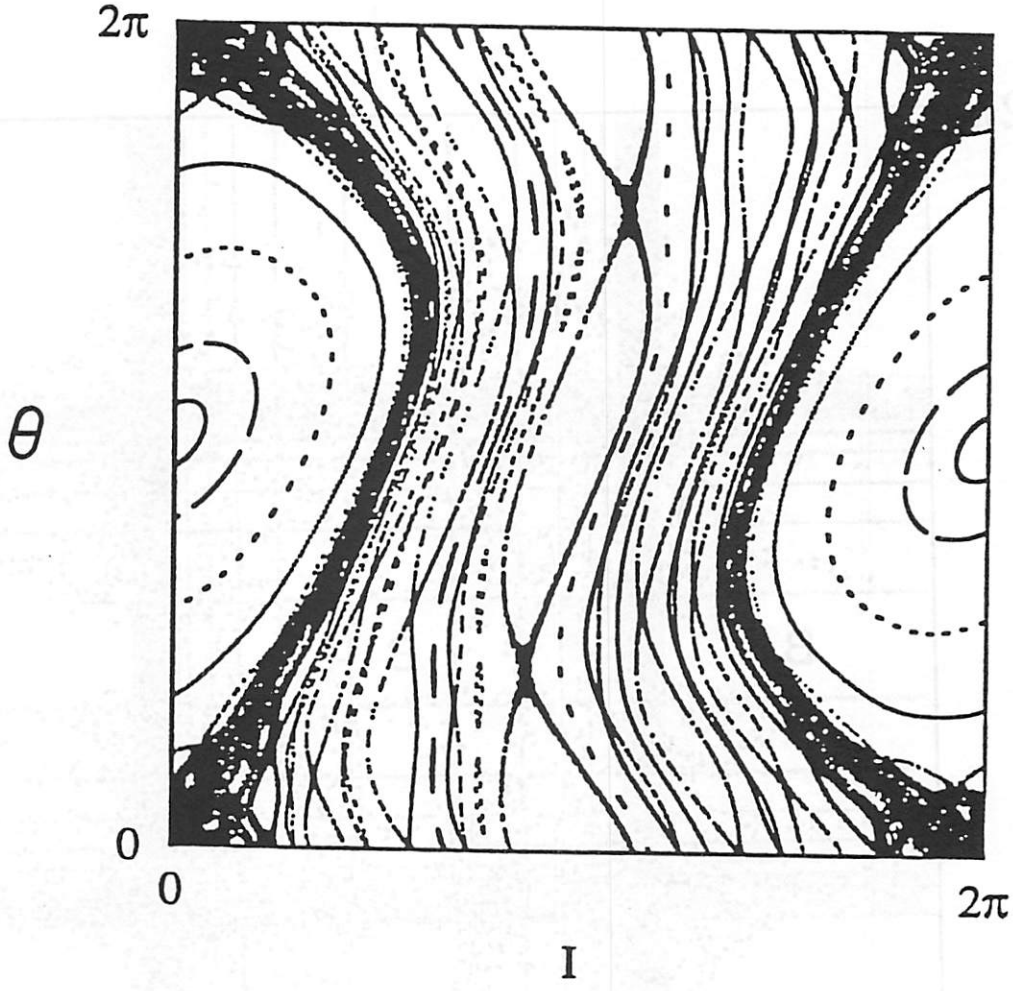

Figure 1

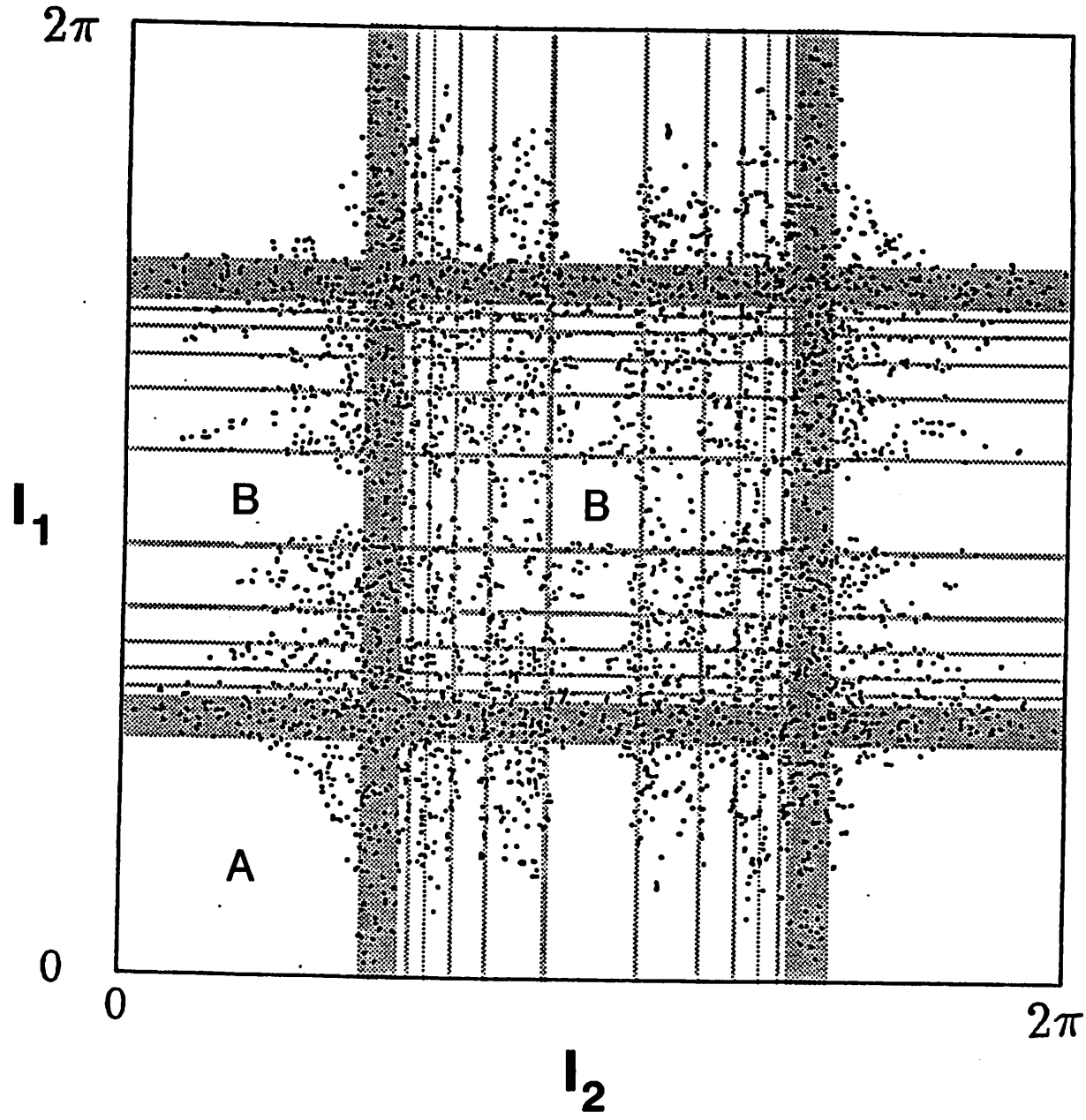

Figure 2

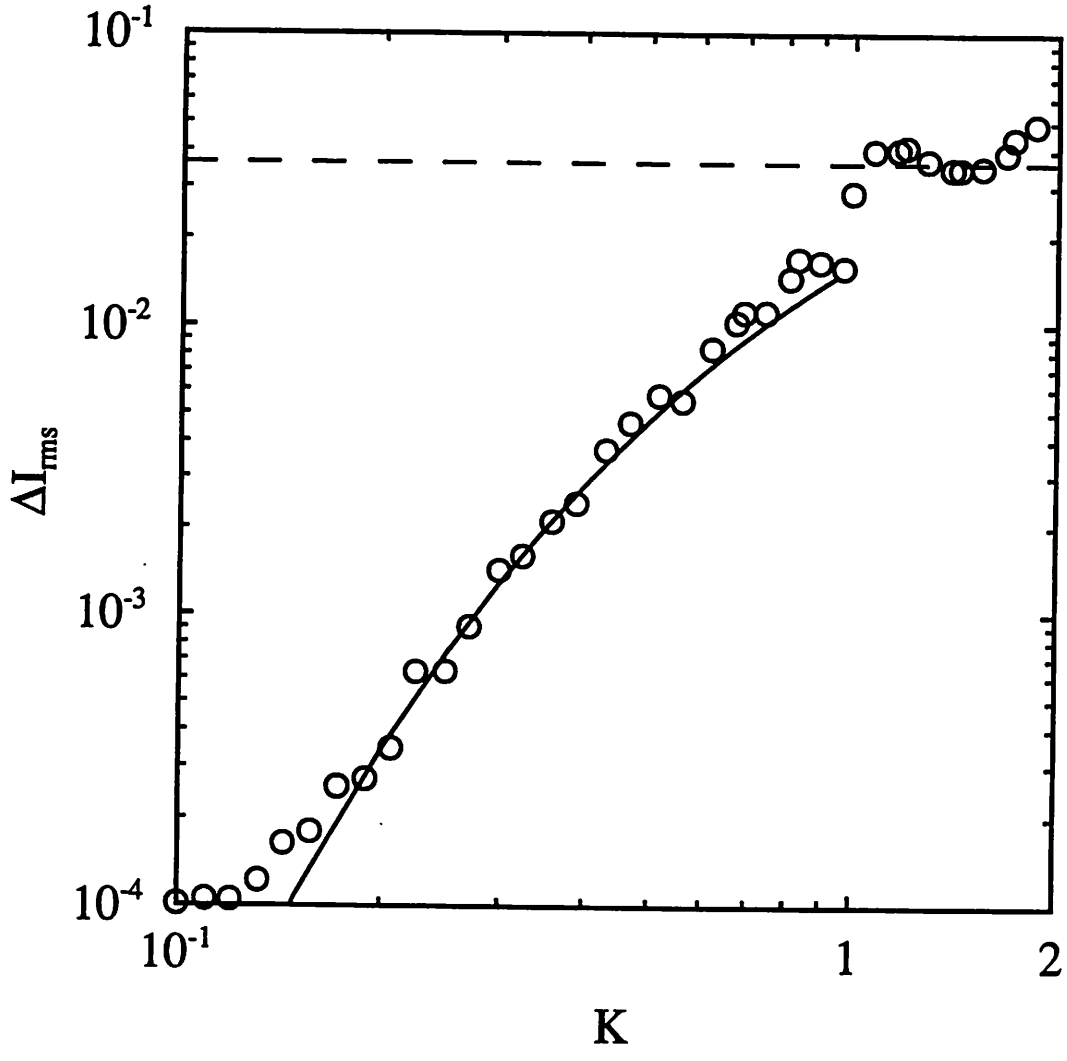

Figure 3

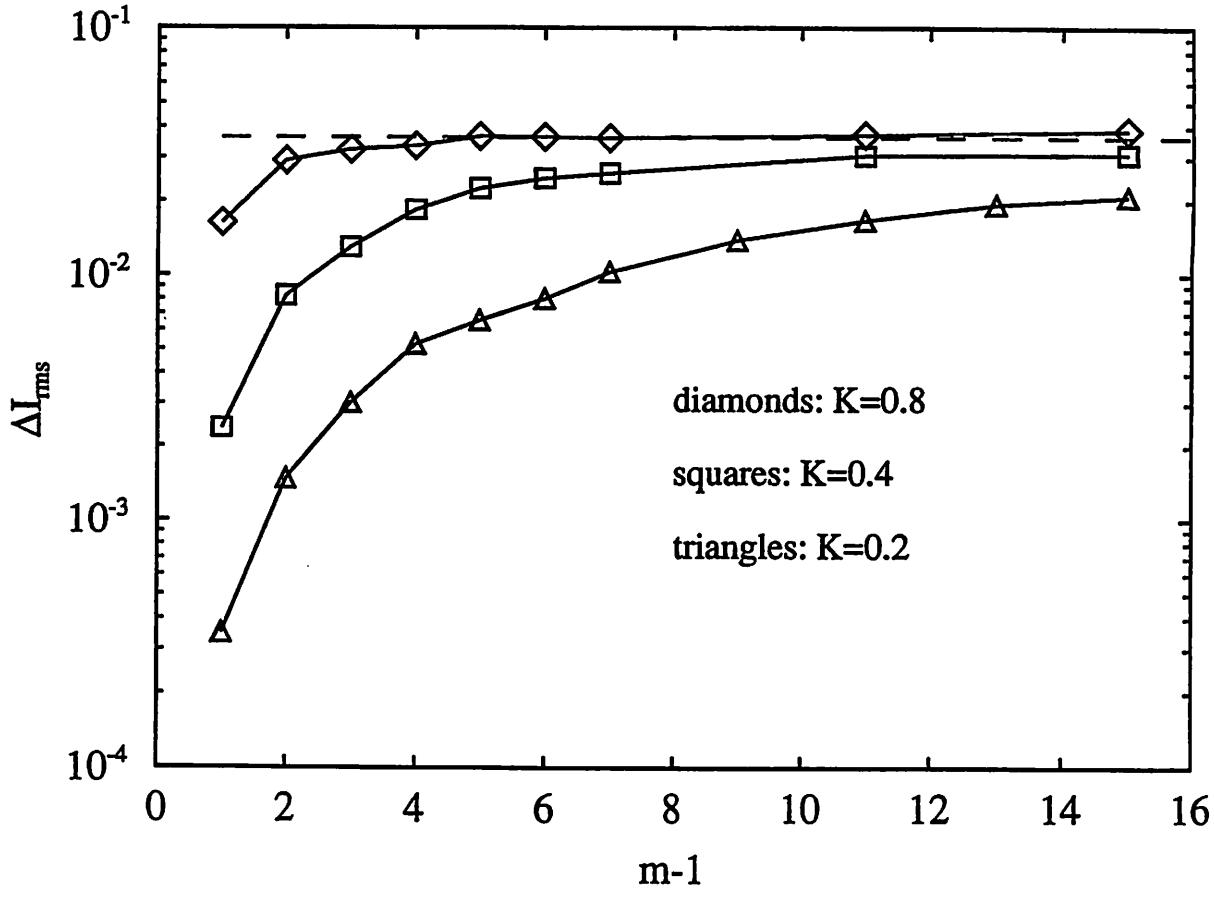
10^{-1}
10^{-2}
10^{-3}
10^{-4}
ΔI_{rms}
diamonds: K=0.8
squares: K=0.4
triangles: K=0.2
0
2
4
6
8
10
12
14
16
m-1

Figure 4

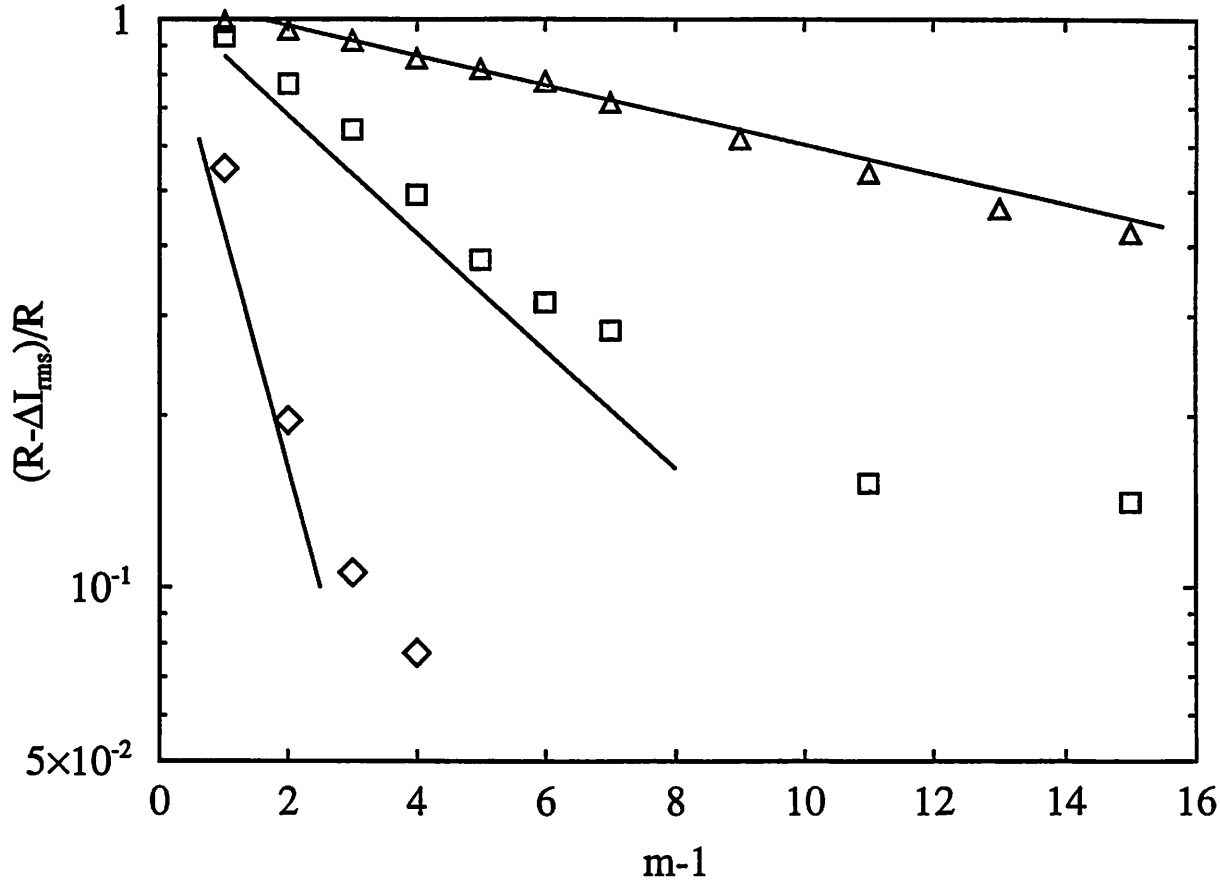

Figure 5

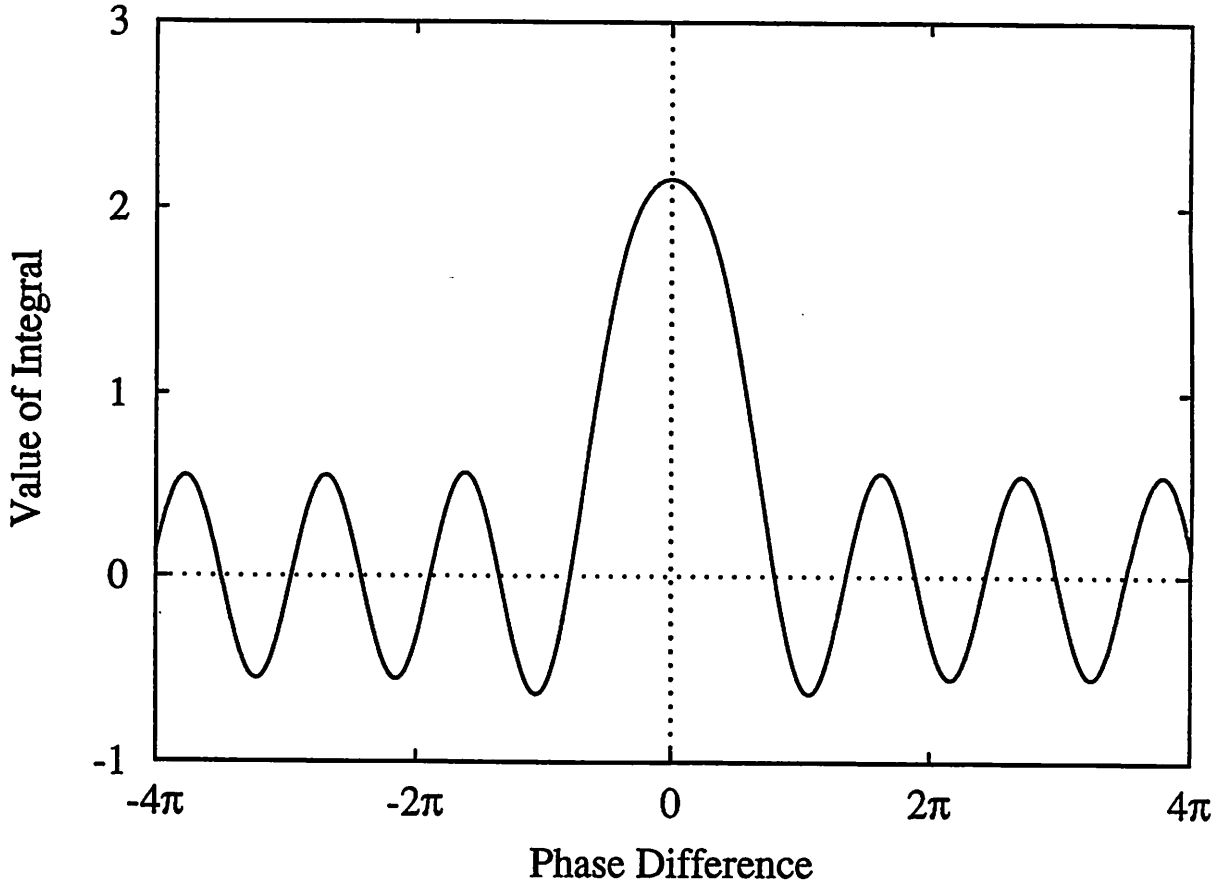

Figure 6

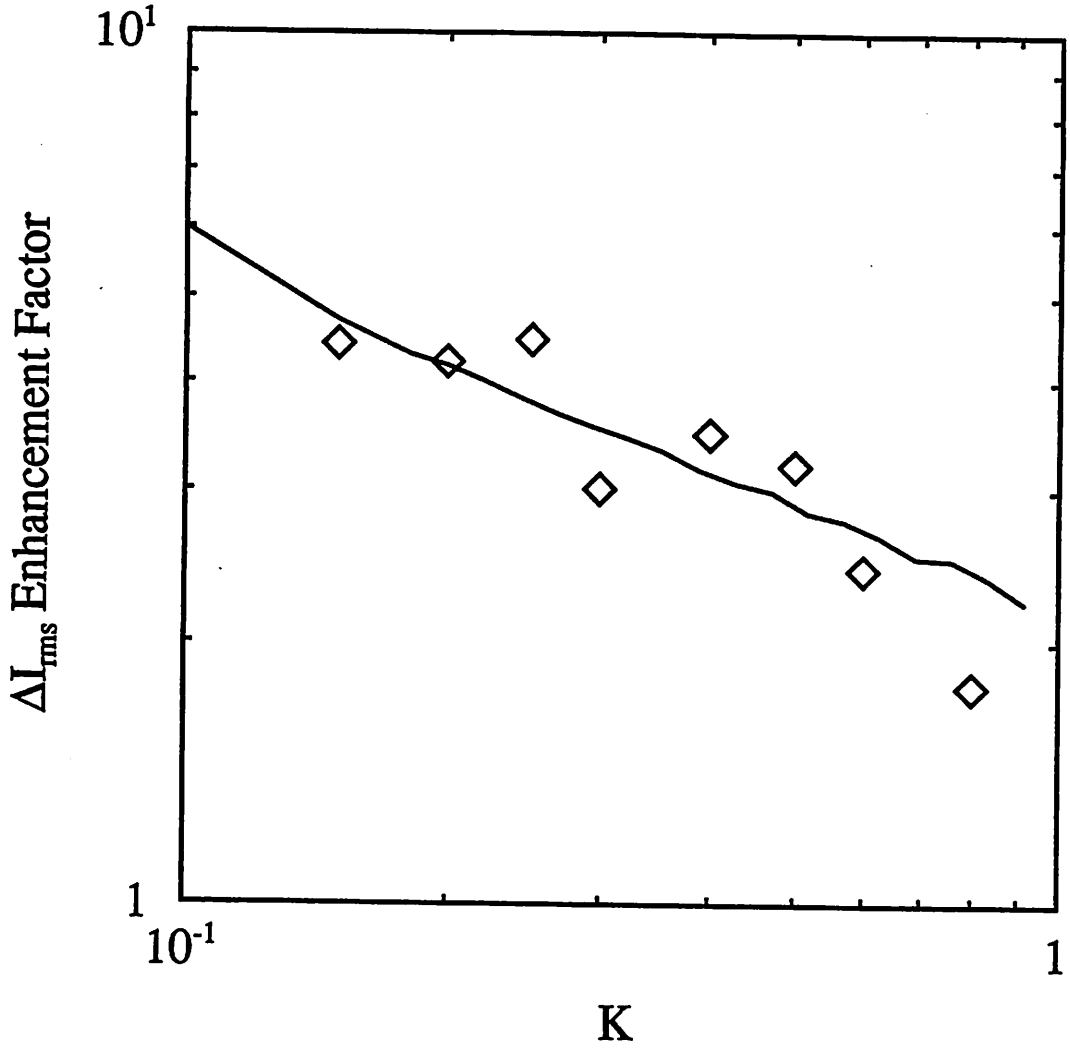

Figure 7

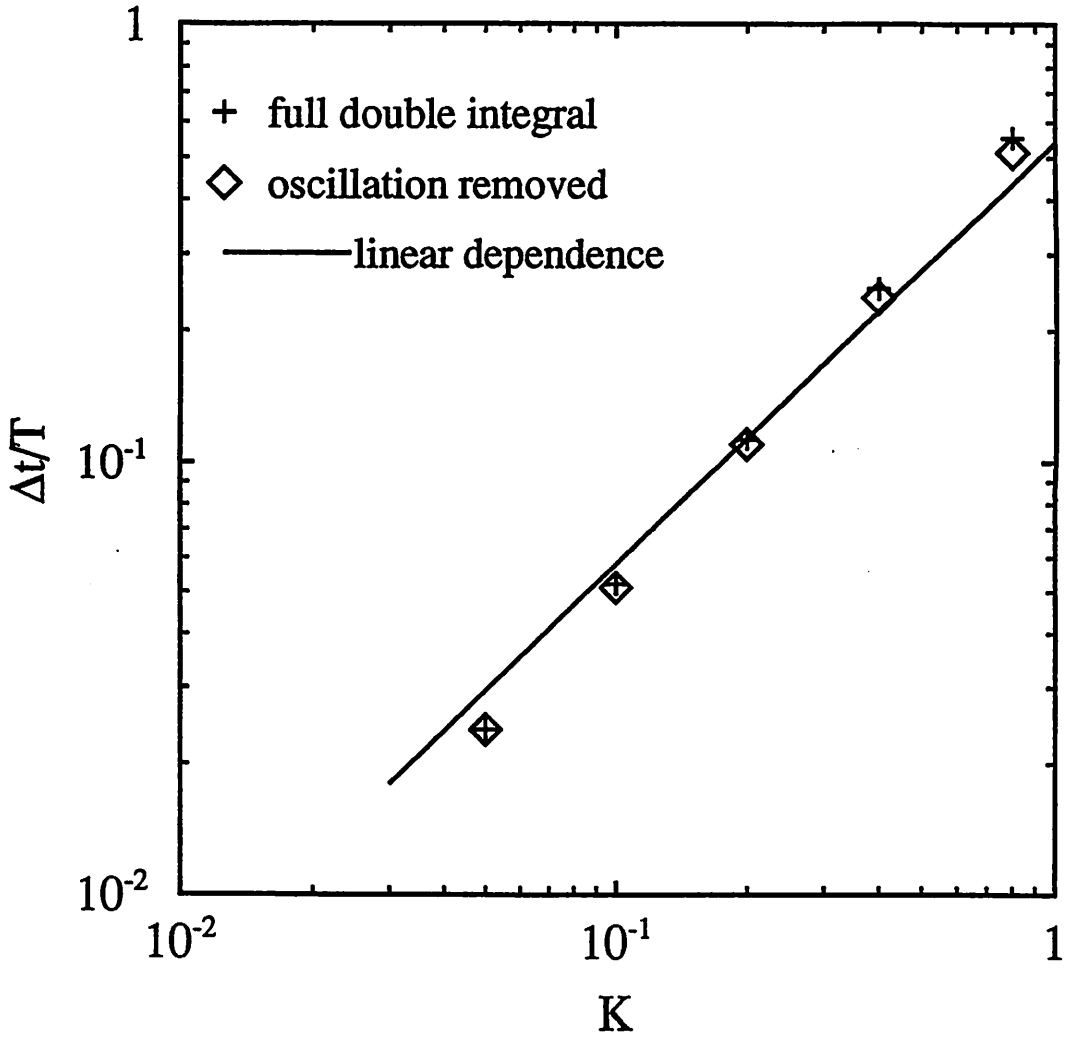
1
+ full double integral
◇ oscillation removed
——linear dependence
Δt/T
10-1
10-2
10-2
10-1
1
K

Figure 8

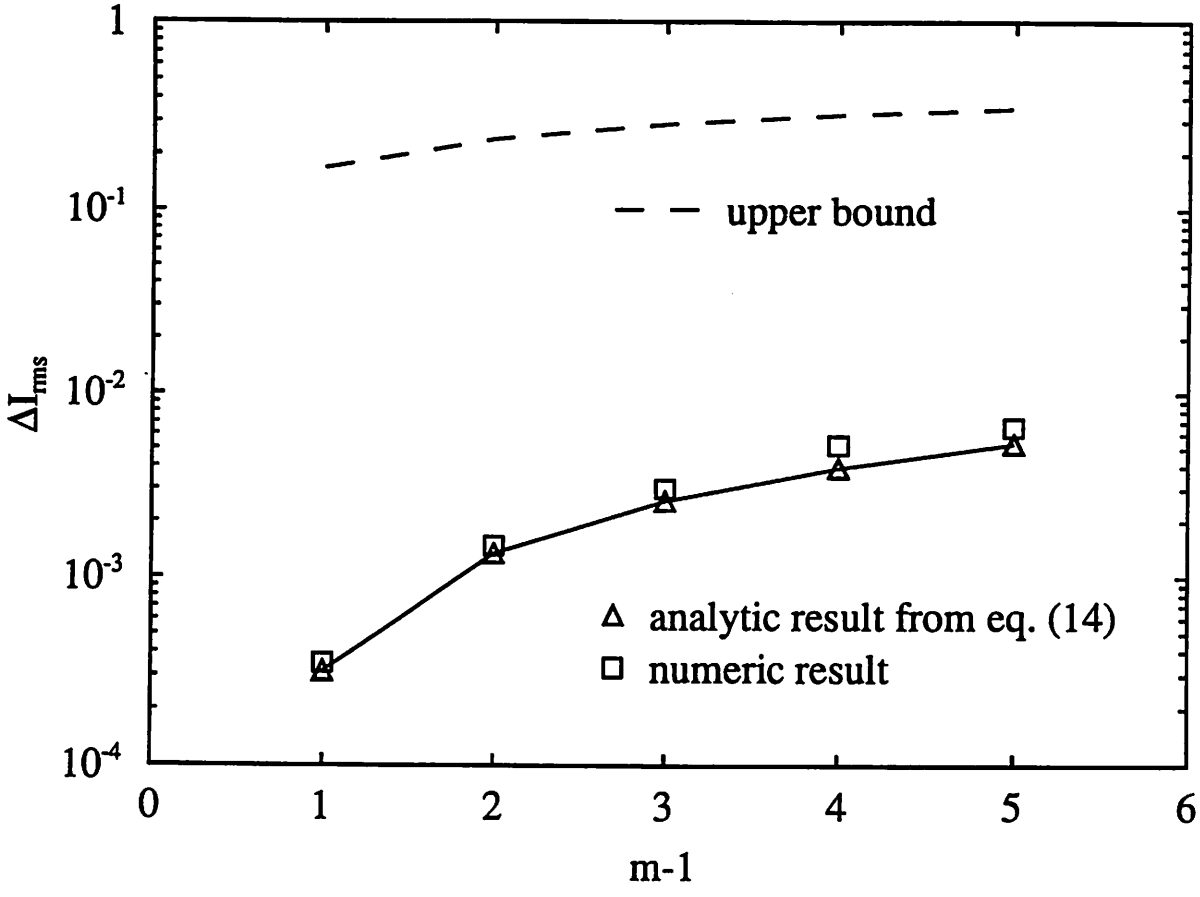
1
10^{-1}
10^{-2}
10^{-3}
10^{-4}
ΔI_{rms}
upper bound
analytic result from eq. (14)
numeric result
0
1
2
3
4
5
6
m-1

Figure 9

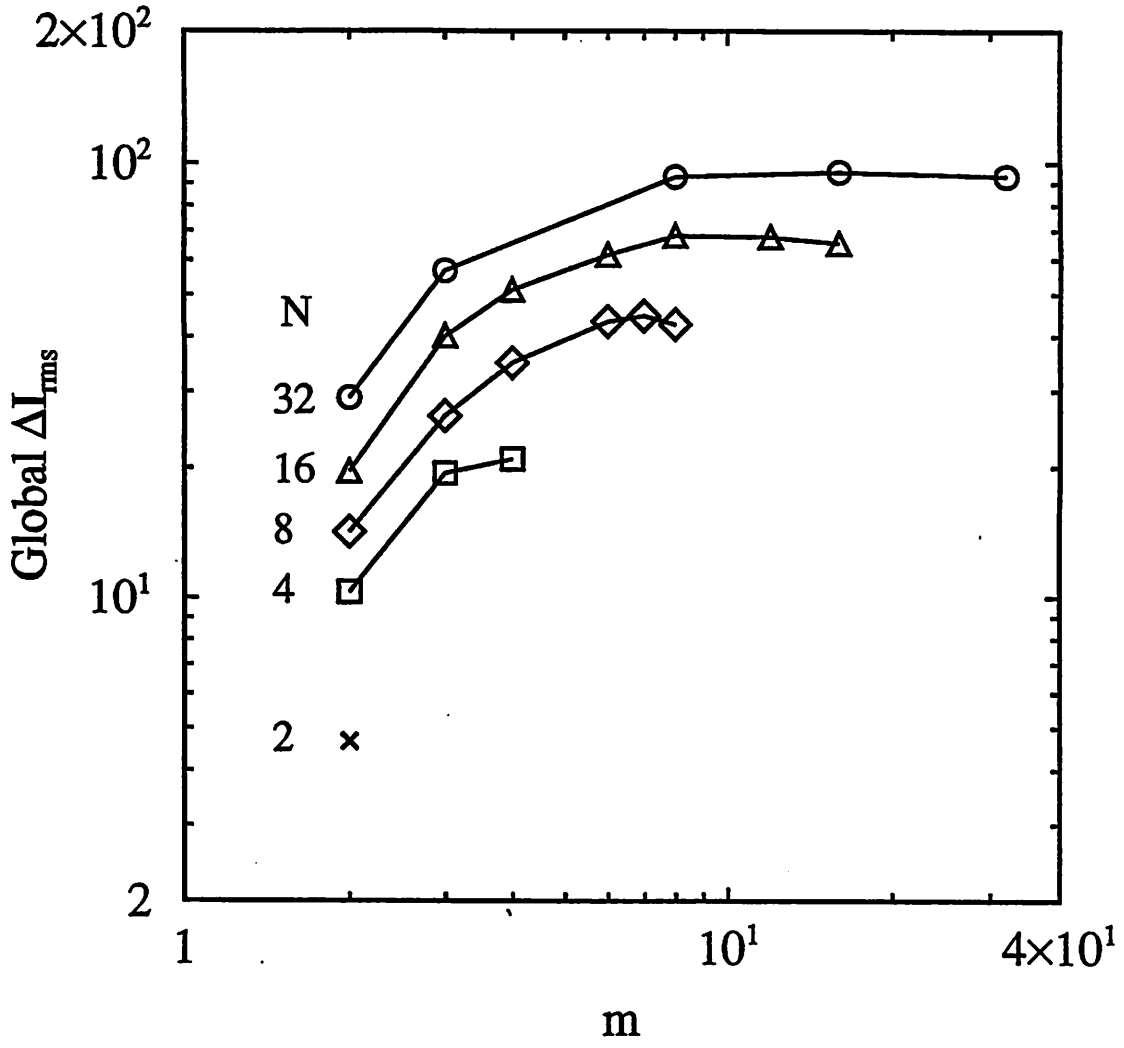

Figure 10

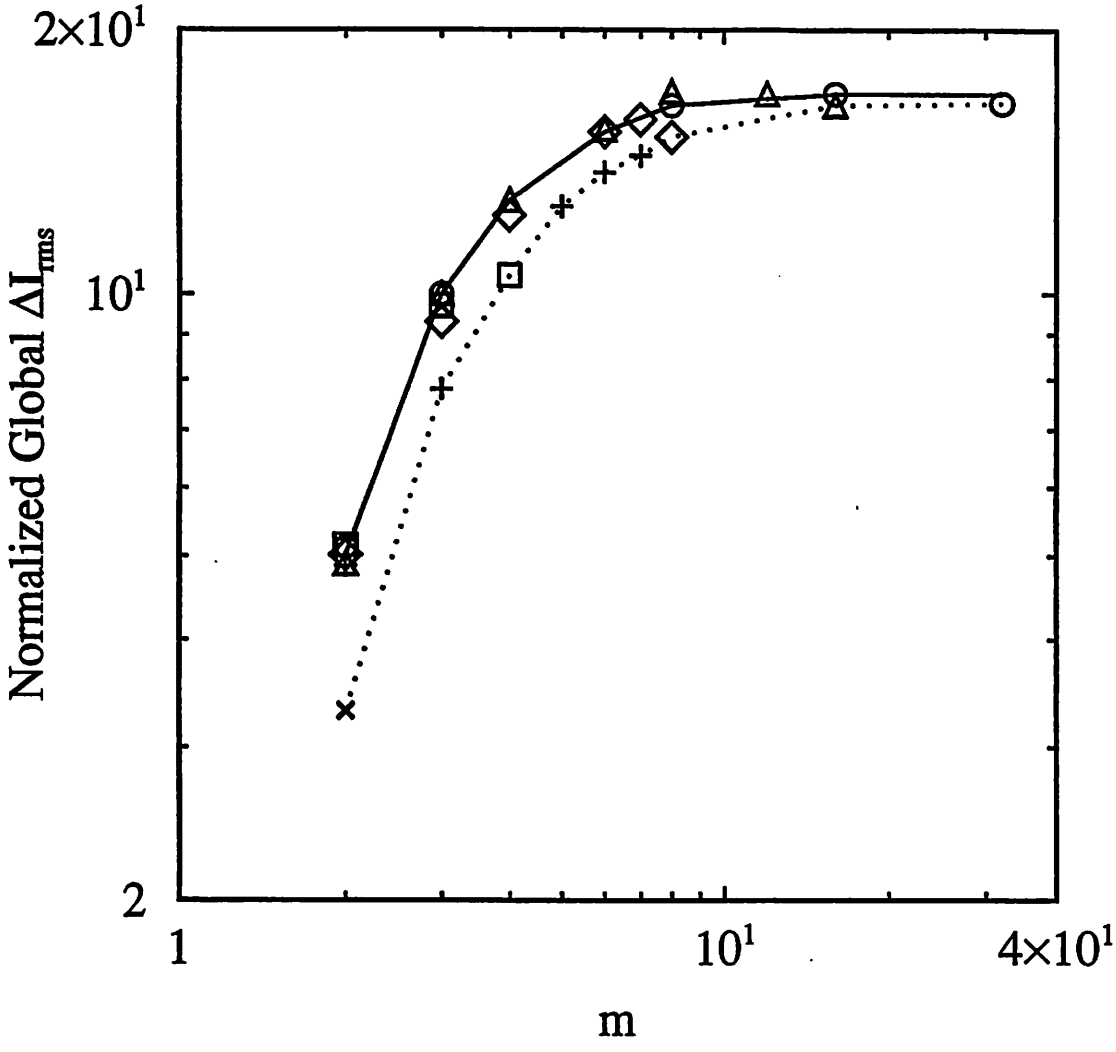

Figure 11

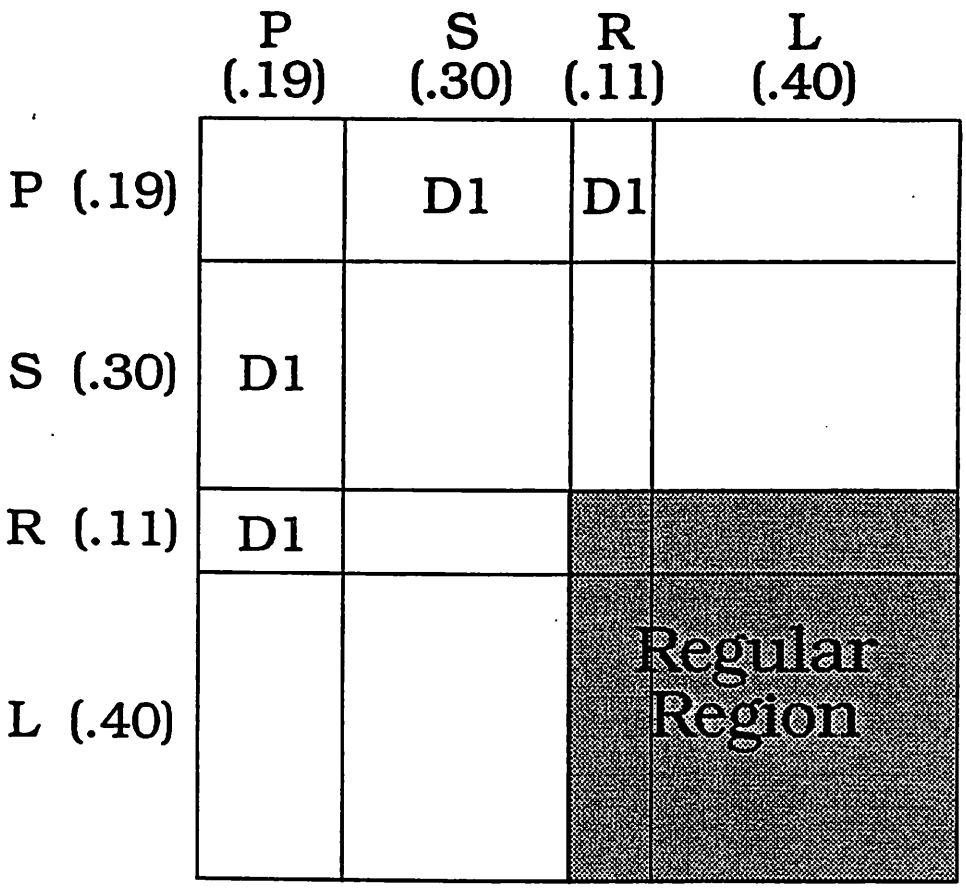

Figure 12